CrossMark

Properties of spray deposited ZnS$_x$Se$_{1-x}$ thin films for photoelectrochemical solar cell application

Nandkishor M. Patil[1] · Santosh G. Nilange[1] · Abhijit A. Yadav[1]

Abstract

The wide band gap II–VI group materials have been extensively studied for optoelectronic applications. The polycrystalline zinc sulphoselenide (ZnS$_x$Se$_{1-x}$) thin films have been spray deposited onto FTO coated glass substrates at temperature of 275 °C. PEC cells were formed with n-ZnS$_x$Se$_{1-x}$ thin films/1 M (NaOH + Na$_2$S + S)/C configuration to study various photoelectrochemical properties. The study signifies n-type conductivity of ZnS$_x$Se$_{1-x}$ thin films. Significant photoelectrochemical response has been witnessed for the films deposited with $x = 0.2$ composition. The flat band potential of -1.09 V has been observed for ZnS$_{0.2}$Se$_{0.8}$ thin film. The junction ideality factors in dark and under radiance are found to be 1.37 and 1.32 respectively. ZnS$_{0.2}$Se$_{0.8}$ thin films produces 268 mV open circuit voltage and 816 µA cm^{-2} short circuit current subsequent to efficiency and fill factor of 1.27% and 0.58 respectively. Spectral response characteristics display a sharp peak at 425 nm for $x = 0.2$, resulting in a band gap of 2.92 eV. These results imply that change in composition 'x' has substantial effect on the photovoltaic properties.

1 Introduction

Binary compounds of group IIB and VIA elements, commonly referred to as II–VI compounds, have technologically important applications. With the exception of HgSe and HgTe (semimetals), they are direct band gap semiconductors with high optical transition probabilities for absorption and emission. They have higher band gap energy than the corresponding III–V compounds due to the larger ionicity in II–VI compounds [1–4]. Among these compounds, only cadmium telluride (CdTe) and zinc selenide (ZnSe) can be prepared in both n- and p-type forms [5]. Thus, the use of thin film II–VI compounds is an economically viable approach to the terrestrial utilization of solar energy [6–8]. In recent times there has been substantial interest in the field of semiconductor electrodes to photoelectrochemical (PEC) solar cell applications [9]. PEC (i.e. solar–liquid junction) has become an economic method for conversion of solar energy into electrical energy, mostly due to the simplicity of formation and quality of the polycrystalline semiconductor–electrolyte junction and hence research into PEC solar cells has gained momentum [10–12].

The interest in the field of II–VI class of semiconducting materials has grown dramatically in recent years owing to their excellent optoelectronic properties and applications in the field of laser diodes, blue light emitting diodes, sensors and photovoltaic devices [13, 14]. Zinc based binary and ternary compound semiconductors ZnSe, ZnS, Zn(O, OH), Zn(O, S), Zn$_{1-x}$Mg$_x$O and ZnS$_x$Se$_{1-x}$ are important members of II–VI semiconductors [15–17]. In literature the solar cell devices using ZnSSe has shown an increased photocurrent as well as efficiency. ZnS$_x$Se$_{1-x}$ is an important ternary material due to their less toxicity, variable band gap from 2.70 to 3.67 eV, which makes it better candidate as a buffer layer for CIS and p-CdTe solar cells [17].

In literature, it has been shown that Zn-based buffer layers of ZnSe, Zn$_{1-x}$Mg$_x$O, Zn(O, S), Zn(O, OH), ZnS$_x$O$_y$H$_z$ are the best alternate layers. Subbaiah and co-workers [18] reported 1.6% power conversion efficiency for ZnS$_{0.5}$Se$_{0.5}$ buffer based thin film prepared using close-spaced evaporation technique [18]. Ojo and Dharmadasa [19] incorporated electrodeposited ZnS, CdS and CdTe thin layers in a graded bandgap solar cell structure of glass/FTO/n-ZnS/n-CdS/n-CdTe/Au with an average conversion efficiency of 14.18%.

Zinc selenide (ZnSe), zinc sulphide (ZnS) and zinc sulphoselenide (ZnS$_x$Se$_{1-x}$) thin films have twofold benefits

✉ Abhijit A. Yadav
aay_physics@yahoo.co.in

1 Thin Film Physics Laboratory, Department of Physics, Electronics and Photonics, Rajarshi Shahu Mahavidyalaya, (Autonomous), Latur, Maharashtra 413512, India

such as non-toxicity and increase the response towards shorter wavelength making them most suitable materials as buffer layer for CIGS solar cells. The performance of thin film solar cells is decided by surface morphology, optical band gap and structure of the thin films. It is possible to tune the optical band gap, the lattice constant and electron affinity of the ZnS_xSe_{1-x} thin films simply by changing composition of S to Se. ZnS_xSe_{1-x} thin films can be grown using a variety of techniques such as molecular beam epitaxy, laser ablation, physical vapour deposition, chemical vapour deposition, chemical bath deposition, electrodeposition, sputtering, brush plating, and spray pyrolysis [20–23]. Amongst these, spray pyrolysis is an attractive technique to grow semiconducting thin films for photovoltaic applications because it is simple, low cost, does not need high quality targets and/or substrates, vacuum free, large area coatings, non-wet, minimum loss of material during deposition, capable of depositing uniform layers [24, 25]. In the present investigation, PEC properties of spray deposited ZnS_xSe_{1-x} thin films with various compositions have been studied and results obtained are discussed.

2 Experimental details

2.1 Preparation of ZnS_xSe_{1-x} thin film electrodes

The AR grade zinc chloride ($ZnCl_2$), thiourea ((NH_2)$_2$CS), and selenourea ((NH_2)$_2$CSe) were used as sources of Zn, S and Se ions respectively. The ZnS_xSe_{1-x} ($x = 0.0, 0.2, 0.4, 0.6, 0.8$ and 1.0) thin films are deposited onto the FTO coated glass substrates via computerised chemical spray pyrolysis technique described elsewhere [26, 27]. All the deposition conditions were kept constant at their optimized values (deposition temperature 275 °C; solution concentration 0.05 M; spray rate 3 cc min^{-1}; deposition time 13–14 min; air as carrier gas with pressure 176,520 N m^{-2} and the distance between substrate and nozzle 30 cm) [28]. However the stock solution was prepared by mixing zinc chloride, thiourea and selenourea together in appropriate proportion to get the Zn:(S + Se) ratio as 1:1. The final spraying solution was prepared by mixing 20 cc of stock solution with 20 cc of isopropyl alcohol. In different set of experiments values of composition parameter (x) were adjusted by varying proportion of thiourea (S) and selenourea (Se). ZnS_xSe_{1-x} thin films are uniform and adhesion of the films onto the substrate was quite good as confirmed using scotch tape test [29].

2.2 Fabrication of ZnS_xSe_{1-x} thin film PEC solar cell

Figure 1 shows the experimental setup used for fabricating ZnS_xSe_{1-x} thin film PEC solar cell. The 1 M polysulphide ($Na_2S + S + NaOH$) is used as a redox electrolyte. PEC cell
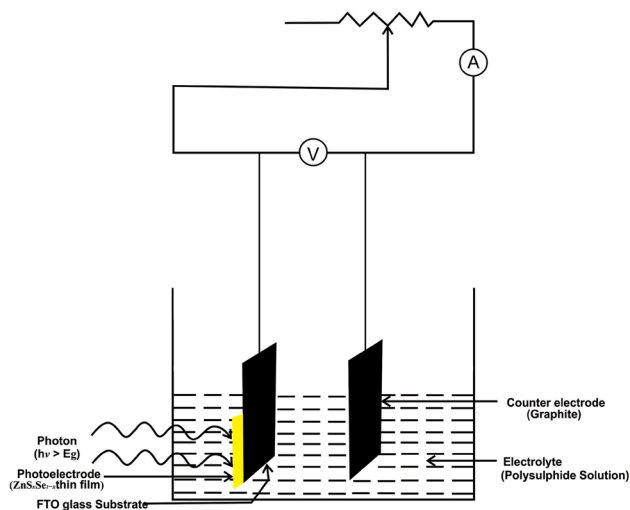
Fig. 1 Experimental setup of n-ZnS_xSe_{1-x} ($0.0 \le x \le 1.0$)/1 M polysulphide/C PEC cell

was made-up in typical three-electrode configuration, Active photo-anodes: n-ZnS_xSe_{1-x}, counter electrode: graphite and reference electrode: SCE. The study of the power output and I–V characteristics were carried out at fixed breaks after waiting for adequate time to equilibrate the system (both in the dark as well as under radiance). Plots of log I versus V were used to calculate the junction ideality factors in dark and under radiance. Mott–Schottky (M–S) graphs were obtained using a LCR (Aplab Model 4912) at built-in frequency of 1 kHz. Power output characteristics for various cell configurations were recorded under a constant illumination intensity of 10 mW cm^{-2}. For estimation of barrier height, the reverse saturation current at various temperatures was noted.

3 Results and discussion

The crystal structures of the as deposited ZnS_xSe_{1-x} thin films have been determined by X-ray diffraction technique. The diffractogram have been depicted elsewhere [28]. X-ray diffraction study confirmed that the polycrystalline ZnS_xSe_{1-x} thin films having a cubic zinc blende structure with a preferential ⟨111⟩ orientation. The shift in the peak ⟨111⟩ direction towards higher 2θ values with increasing sulfur concentration confirmed the formation of a solid solution. The crystallite size is observed to be in the range 18–28 nm. Using energy dispersive X-ray spectroscopy, the formation of nearly stoichiometric ZnS_xSe_{1-x} thin films is confirmed. The optical band gap increased from 2.84 to 3.57 eV when the composition of the ZnS_xSe_{1-x} is changed. The thin films are found to be semiconducting in nature from electrical resistivity measurement [28]. To study the

influence of composition variation in ZnS_xSe_{1-x} thin film based electrodes in PEC solar energy conversion, photo-electrochemical measurements were carried out for $x = 0.0$, 0.2, 0.4, 0.6, 0.8 and 1.0 respectively underneath dark and illumination of white light of intensity 10 mW cm^{-2}.

3.1 Type of conductivity

The PEC cells with configuration of ZnS_xSe_{1-x}/1 M polysulphide/graphite are designed in order to test the type of conductivity revealed by ZnS_xSe_{1-x} thin films. When ZnS_xSe_{1-x} semiconductor electrode is in contact with redox electrolyte (polysulphide) in dark, electronic equilibrium is developed between the ZnS_xSe_{1-x} electrode and electrolyte. Even in dark, ZnS_xSe_{1-x} thin film based PEC cells showed small dark voltage (open circuit voltage) due to difference between two half potentials in ZnS_xSe_{1-x} thin film based PEC cell. When this junction is illuminated with white light the open circuit voltage is found to enhance with negative polarity towards ZnS_xSe_{1-x} thin films indicating n-type of conductivity [30].

3.2 Capacitance–voltage (C–V) characteristics

The semiconductor/electrolyte junction has significant role in the applications of solar energy conversion. The detailed analysis of semiconductor/electrolyte interface can be obtained from the review by Pandey and co-workers [31] and mechanism of charge transfer across this active interface can be properly understood in literature [32–35]. The C–Vs offer important evidence about the type of conductivity, flat band potential (V_{fb}) and the donor concentration (N_D). In present investigation, n-ZnS_xSe_{1-x}/polysulphide interfaces are formed for a series of PEC cell configurations and the Schottky capacitance at a 1 Vpp–1 kHz ac signal was measured as a function of the applied dc bias from -0.6 to 0.6 V. The unpinned band edges move with applied bias, making the n-ZnS_xSe_{1-x} electrode behave similar to a metal electrode in that changes in applied bias occur across the Helmholtz layer rather than across the n-ZnS_xSe_{1-x} space charge layer. Thus the potential drop across the Helmholtz layer is important to the biasing requirements of a PEC and is directly affected by the chemisorption of ions at the n-ZnS_xSe_{1-x}/polysulphide interface [33]. Figure 2 displays the M–S graphs for n-ZnS_xSe_{1-x}/polysulphide/C system in dark. The V_{fb}, was determined on the voltage-axis (at $1/C_s^2 = 0$) according to familiar M–S relation [35],

$$\frac{1}{C_s^2} = \left(\frac{2}{\varepsilon_0 \, \varepsilon_s \, qN_D} \right) \left[V - V_{fb} - \left(\frac{kT}{q} \right) \right] \quad (1)$$

where C_s is the space charge capacitance, V_{fb} is the flat band potential, V is electrode potential, ε_0 is the permittivity of
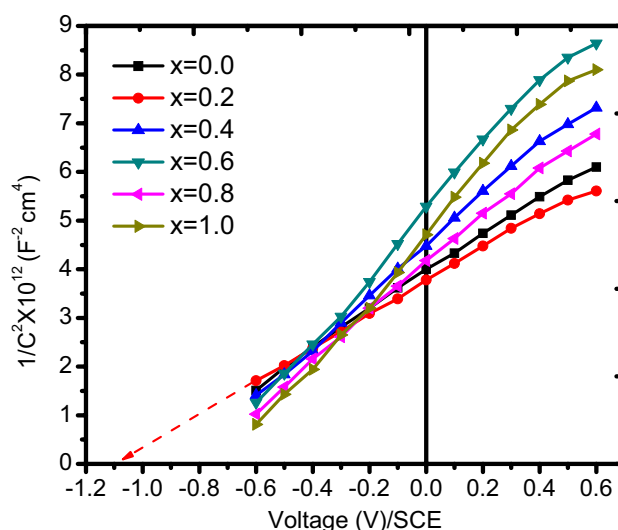

Fig. 2 Mott–Schottky plots of n-ZnS_xSe_{1-x} $(0.0 \leq x \leq 1.0)$/1 M polysulphide/C PEC cell at frequency f = 1 kHz
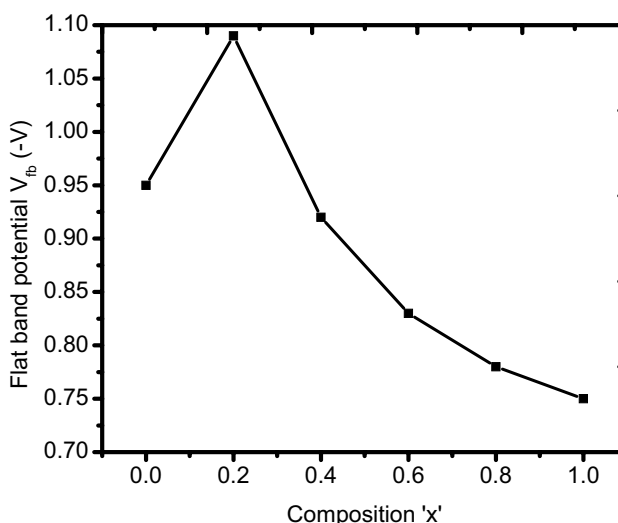

Fig. 3 Variation of flat band potential (V_{fb}) with composition for spray deposited ZnS_xSe_{1-x} $(0.0 \leq x \leq 1.0)$ thin film based PEC cells

free space, ε_s is the static permittivity of the semiconductor, N_D is donor concentration and q is the charge on electron. The variation of V_{fb} as a function of composition 'x' is shown in Fig. 3. It is observed that the V_{fb} increases from -0.95 to -1.09 V with increase in composition 'x' from 0.0 to 0.2, and decreases further to -0.75 V with increase in composition from 0.2 to 1.0. The V_{fb} is typically determined by the properties of the n-ZnS_xSe_{1-x}/polysuphide junction and of the space-charge layer, at $x = 0.0$ and 0.2 the variation of V_{fb} could in principle be caused by changes in the Helmholtz layer capacitance [36]. The different parameters including non-planar interface, surface roughness, and ionic

Table 1 Important PEC parameters of spray deposited ZnS_xSe_{1-x} ($0.0 \leq x \leq 1.0$) thin films

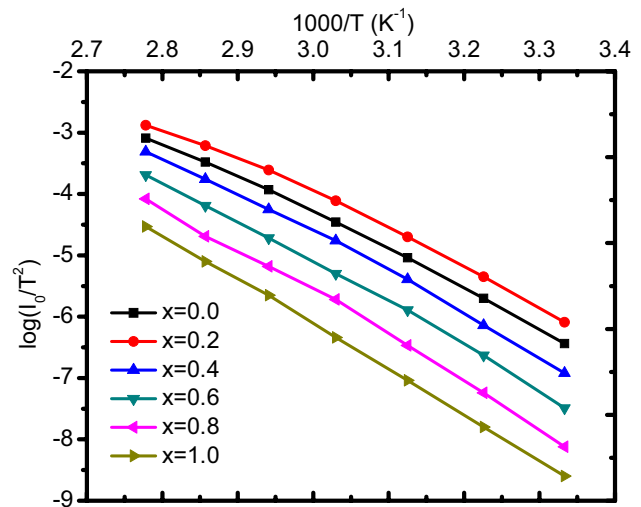| Composition	n_d	n_L	I_{sc} ($\mu A\ cm^{-2}$)	V_{oc} (mV)	η (%)	FF	Φ_b (eV)	R_s (Ω)	R_{sh} (kΩ)	N_D ($\times 10^{19}\ cm^{-3}$)	D (nm)	E_g (eV)
ZnSe	1.52	1.36	688	258	1.01	0.57	0.55	70	4.00	2.58	22	2.76
$ZnS_{0.2}Se_{0.8}$	1.37	1.32	816	268	1.27	0.58	0.54	57	3.43	2.87	28	2.92
$ZnS_{0.4}Se_{0.6}$	1.63	1.41	566	254	0.77	0.54	0.60	76	4.50	2.35	26	3.10
$ZnS_{0.6}Se_{0.4}$	1.74	1.46	472	228	0.55	0.51	0.63	99	5.02	2.21	23	3.31
$ZnS_{0.8}Se_{0.2}$	1.86	1.54	390	206	0.39	0.48	0.65	108	5.75	2.07	21	3.42
ZnS	2.03	1.65	311	188	0.27	0.47	0.67	118	6.50	1.89	18	3.54

n_d junction ideality factor in dark, n_L junction ideality factor under illumination, I_{sc} short circuit current, V_{oc} open circuit voltage, η efficiency, FF fill factor, Φ_b barrier height, R_s series resistance, R_{sh} shunt resistance, N_D donor concentration, D crystalline size, E_g band gap energy
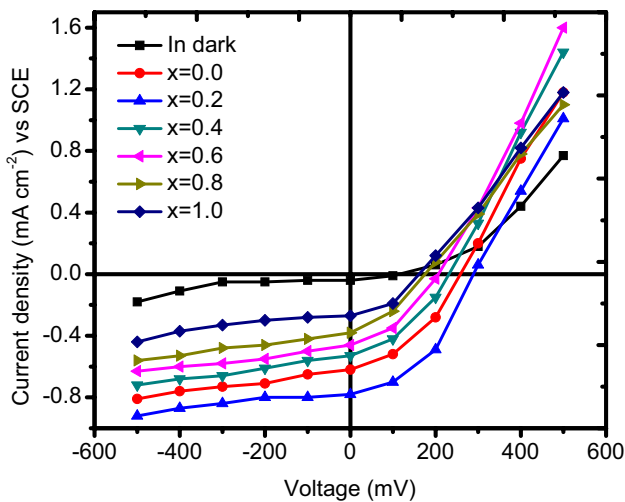
Fig. 4 Current–voltage characteristics of n-ZnS_xSe_{1-x} ($0.0 \leq x \leq 1.0$) thin films/1 M polysulphide/C PEC cells in dark and under illumination

Fig. 5 Plots of log I_0/T^2 versus 1000/T for spray deposited ZnS_xSe_{1-x} ($0.0 \leq x \leq 1.0$) thin film based PEC cells

adsorption on the n-ZnS_xSe_{1-x} surface also play a crucial role in determination of V_{fb} [35]. The values of N_D are given in Table 1.

3.3 Current–voltage (I–V) characteristics

Figure 4 exhibits I–V curves for n-ZnS_xSe_{1-x} thin films/1 M polysulphide/C PEC cells in dark and under illumination. All the electrodes had similar characteristics in the dark and one of the representative characteristics obtained with x = 0.2 in ZnS_xSe_{1-x} is shown in Fig. 4. When n-ZnS_xSe_{1-x} thin films/1 M polysulphide/C junctions are illuminated the currents and voltages are developed by the generating excessive mobile charge carriers through light absorption. An efficient separation of electron–hole pairs happens in the space charge layer underneath the n-ZnS_xSe_{1-x}/polysulphide contact. After illumination of the junction, I–V curve shifts in the IVth quadrant suggesting that the PEC cell can work as electricity generator.

The graphs of logI versus V under illumination for n-ZnS_xSe_{1-x} ($0.0 \leq x \leq 1.0$) thin films show linear behavior (figures are not given). The junction ideality factors in dark and under illumination are estimated from the slope of the linear regions of the logI versus V curves using well-known diode equation given elsewhere [37]. The estimated junction ideality factors n_d and n_L are given in Table 1. It is observed that these values are close to 1 suggesting formation of good quality junction. The higher values of n_L is suggestive of the impact of series resistance and the carrier recombination at the n-ZnS_xSe_{1-x}/polysulphide interface [38, 39].

3.4 Barrier-height measurements

The barrier-height also known as built-in-Potential (Φ_b), was obtained by measuring the reverse saturation current 'I_0' flowing through the n-ZnS_xSe_{1-x} thin films/1 M polysulphide/C junction in the temperature range 363–303 K. Figure 5 is a current–temperature profile of

ZnS_xSe_{1-x} electrode in polysulfide electrolyte. The reverse saturation current was observed to increase with increase in temperature of PEC cell. This may be due to the fact that with increased temperature of PEC cell provides more charge carriers resulting in increased reverse saturation current. Figure 5 shows a graph of log I_0/T^2 versus 1000/T for ZnS_xSe_{1-x} electrode. The observed nonlinearity of plots in high temperature regions is accredited to Pool-Frankel type of conduction mechanism. Similar behavior has been witnessed by Mahapatra and Dubey [40] for CdS–CdSe electrodes. The reverse saturation current flowing through junction depends on the temperature and relation between temperature and this reverse current is [39],

$$I_0 = AT^2 \exp(\Phi_b/kT) \qquad (2)$$

where A denotes Richardson constant, k is the Boltzmann constant, and Φ_b is the junction barrier height (in eV). The values of barrier height are given Table 1. It is noted that the junction barrier height value decreases from 0.55 to 0.54 eV as the composition 'x' increased from 0.0 to 0.2 and it was minimum 0.54 eV for $x = 0.2$, which further increased to 0.67 eV for $x = 1.0$.

3.5 Photovoltaic power output characteristics

Figure 6 displays the photocurrent density ($\mu A\ cm^{-2}$) against photovoltage (mV) characteristics i.e. power output characteristics curve of the cell fabricated with ZnS_xSe_{1-x} ($0.0 \leq x \leq 1.0$) thin films. The PEC cell performances as a function of composition of ZnS_xSe_{1-x} films are presented in Table 1. Figure 7 displays the variation curve of I_{sc} and V_{oc} as a function of composition 'x' for spray deposited ZnS_xSe_{1-x} thin films. As can be seen from Table 1 and Fig. 7, I_{sc} and V_{oc} values are both increasing with the increase in composition
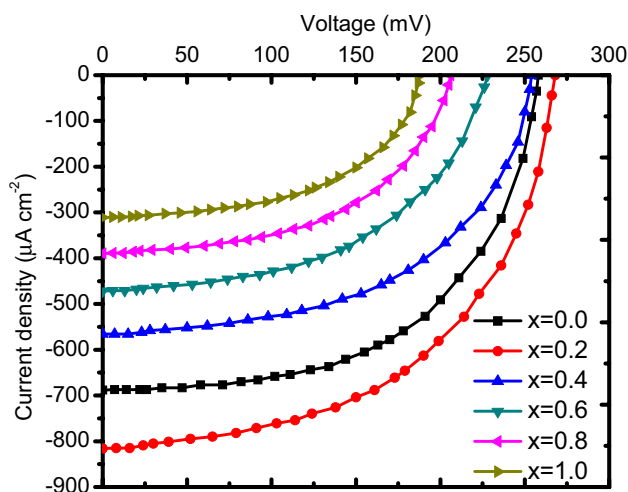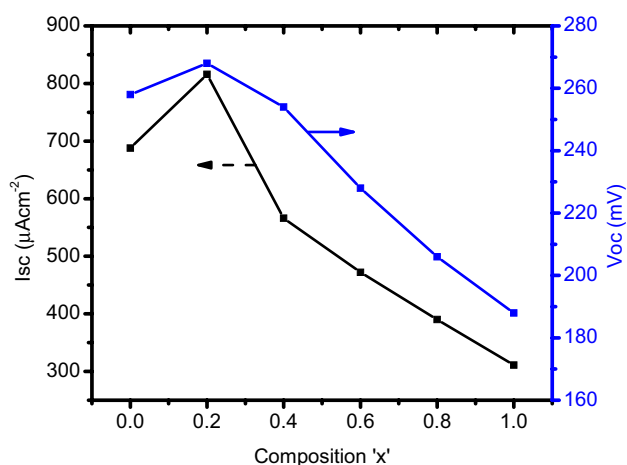
Fig. 7 Variation I_{sc} and V_{oc} with composition 'x' for spray deposited ZnS_xSe_{1-x} ($0.0 \leq x \leq 1.0$) thin film based PEC cells

from 0.0 to 0.2. The measured I_{sc} value of 688 $\mu A\ cm^{-2}$ for the cell with $x = 0.0$ increases to 816 $\mu A\ cm^{-2}$ for $x = 0.2$. Similarly, the V_{oc} value also increases from 258 to 268 mV. This enhancement is due to the structural rearrangement and higher degree of crystallinity obtained in the samples with $x = 0.2$. Consequently, the charge scattering at grain boundaries falls and I_{sc} is improved. The V_{oc} on the other hand upsurge with the increase in composition as a mixture of two effects, i.e. greater hole diffusion velocity and decreased recombination of charge carriers between the photo-reduced polysuphide and injected holes [41]. The former is probably due to better connection between the particles and the latter is due to the lowered surface defects; both arise simply because of improved crystallinity for $x = 0.2$. Further increments in the composition from $x = 0.2$ in ZnS_xSe_{1-x} produce dramatically downfall in both I_{sc} and V_{oc} because the increase of the recombination processes and trapping effects into ZnS_xSe_{1-x}, subtracting electrons to the external circuit. For higher values of 'x' pinning of Fermi level may decrease V_{oc}. The lower magnitudes of short circuit current for higher values of 'x', on the other hand, can be correlated to the increased recombination mechanism not only at the grain boundaries but also at the electrode–electrolyte interface. At higher 'x' values, the role of surface states may also become dominant causing a decrease in both open circuit voltage and short circuit current. These findings revealed that composition $x = 0.2$ produces better films which can be utilized as electrodes in PEC cells.

The performance of a PEC cell is described with parameter fill factor (FF) and photovoltaic efficiency η (%), which can be calculated from photovoltaic power output characteristics using relation given elsewhere [42]. The FF values obtained are listed in Table 1. It shows that fill factor is maximum 0.58 for $ZnS_{0.2}Se_{0.8}$ thin film. From Table 1, it is clear that the FF of the cells increases with increasing

Fig. 6 Power output characteristics of spray deposited ZnS_xSe_{1-x} ($0.0 \leq x \leq 1.0$) thin film based PEC cells

composition upto $x = 0.2$ and decrease further. The increase in FF could be ascribed to the reduction in the penetration of the redox couple into the pores of photocathode layer due to higher densification of the films at $x = 0.2$.

From Table 1 it is clear that efficiency is maximum 1.27% for $ZnS_{0.2}Se_{0.8}$ thin film due to large grain sizes as compared to other films deposited with different compositions. The overall efficiency is larger for $ZnS_{0.2}Se_{0.8}$, since a wider range of visible light is absorbed in that case. The differences in efficiency between the other compositions were more pronounced in the case of ZnS. The overall low power conversion efficiency of PEC cell is probably due to large series resistance and interface states which are responsible for recombination mechanism [43].

The series resistance (R_s) and shunt resistance (R_{sh}) for n-ZnS_xSe_{1-x} thin films/1 M polysulphide/C PEC cells were assessed from the slopes of power output characteristics at $I = 0$ and $V = 0$, respectively using the following relation [42],

$$\left(\frac{dI}{dV}\right)_{I=0} \cong \left(\frac{1}{R_s}\right) \qquad (3)$$

$$\left(\frac{dI}{dV}\right)_{V=0} \cong \left(\frac{1}{R_{sh}}\right) \qquad (4)$$

The series and shunt resistances for ZnS_xSe_{1-x} thin film deposited with different compositions 'x' were listed in Table 1. The minimum values of series and shunt resistance are found to be 57 Ω and 3.43 kΩ respectively for $ZnS_{0.2}Se_{0.8}$ thin films ($x = 0.2$).

3.6 Spectral response studies

The photoresponse was further studied with the spectral response measurements in the PEC cells, as shown in Fig. 8. The spectral response shows that only an n-type photocurrent is produced in the entire spectral range (300–600 nm) indicating formation of good ZnS_xSe_{1-x} electrode based PEC cell. From Fig. 8 it is seen that for all the prepared samples I_{sc} rises with λ and attain maximum value at a particular wavelength and diminishes afterwards with further increase in λ. It is noticed that the I_{sc} reaches maximum at different wavelengths according to the composition (x) in ZnS_xSe_{1-x}. Out of all the prepared samples only $ZnS_{0.2}Se_{0.8}$ thin films possesses high spectral sensitivity at wavelength 425 nm giving an optical energy gap of 2.92 eV. This value is adjacent to the band gap energy 2.98 eV for $ZnS_{0.2}Se_{0.8}$ examined at room temperature in optical absorption studies [28] using UV–Vis spectrophotometer (SHIMADZU UV-1700). The decay in photocurrent value on the longer wavelength side of may be accredited to the transition between defect
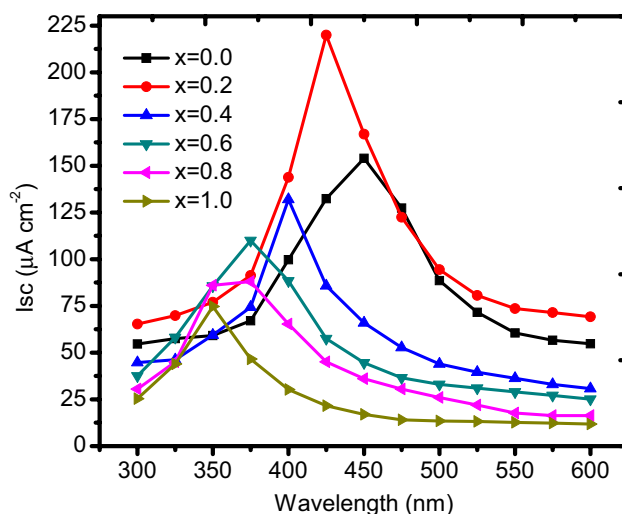
Fig. 8 Spectral response curves for spray deposited n-ZnS_xSe_{1-x} ($0.0 \le x \le 1.0$)/1 M polysulphide/C PEC cells

levels and non-optimized thickness. The optical energy gap values obtained are given in Table 1.

4 Conclusion

In summary, we have successfully synthesized polycrystalline ZnS_xSe_{1-x} electrodes onto conducting FTO coated glass substrates via simple, convenient and cost effective chemical spray pyrolysis technique. The effects of composition variations in ZnS_xSe_{1-x} thin films on the photoelectrochemical features of PEC cells are also explored. All the electrodes are of n-type. The flat band potential V_{fb} changes from −0.75 to −1.09 V and is reached its maximum for the PEC cell with $ZnS_{0.2}Se_{0.8}$ photoelectrode. From I–V characteristics the higher values of n_L is suggestive of the influence of series resistance and the carrier recombination at the n-ZnS_xSe_{1-x}/polysulphide interface. The barrier height is observed to be in the range of 0.54–0.67 eV. The maximum photo conversion efficiency and FF are found to be 1.27% and 0.58 respectively for $ZnS_{0.2}Se_{0.8}$ PEC cell. The series and shunt resistance are found to be 57 Ω and 3.43 kΩ respectively for $ZnS_{0.2}Se_{0.8}$ based PEC cell. All prepared samples showed a high spectral sensitivity. These resulting performances of ZnS_xSe_{1-x} thin films electrodes are paving the way for the improvement of a new generation of PEC cells with analogous efficiencies.

References

1. E. Abdel-Fattah, I.A. Elsayed, T. Fahmy, J. Mater. Sci.: Mater. Electron. **29**, 19942–19950 (2018)

2. F.J. Ochoa-Estrella, A. Vera-Marquina, I. Mejia, A.L. Leal-Cruz, M.I. Pintor-Monroy, M. Quevedo-López, J. Mater. Sci.: Mater. Electron. **29**, 20623–20628 (2018)

3. M.A. Khan, R. Singh, S. Mukherjee, Review of II-VI based compounds for transistor applications, reference module in Materials Science and Materials Engineering (2018)

4. W. Mahmood, J. Ali, I. Zahid, A. Thomas, A. ul Haq, Optik **158**, 1558–1566 (2018)

5. P. Gu, X. Zhu, J. Li, H. Wu, D. Yan, J. Mater. Sci.: Mater. Electron. **29**, 14635–14642 (2018)

6. S. Yılmaz, İ Polat, M. Tomakin, S.B. Töreli, T. Küçükömeroğlu, E. Bacaksız, J. Mater. Sci.: Mater. Electron. **29**, 14774–14782 (2018)

7. B. Wang, B. Li, T. Shen, M. Li, J. Tian, J. Energy Chem. **27**, 736–741 (2018)

8. D.A. Barlow, J Crystal Growth **479**, 93–97 (2017)

9. M. Gratzel, Philos. Trans. R. Soc. A **365**, 993–1005 (2007)

10. M. Shirazi, M.R. Toroghinejad, R. Sabet Dariani, M.T. Hosseinnejad, J. Mater. Sci.: Mater. Electron. **29**, 10092–10101 (2018)

11. S. Tiwaria, S. Tiwari, Sol. Energy Mater. Sol. Cells **90**, 1621–1628 (2006)

12. G. Hodes, Nature **285**, 29–30 (1980)

13. M. Isshiki, J. Wang, *Wide-Bandgap II-VI Semiconductors: Growth and Properties, Springer Handbook of Electronic and Photonic Materials* (Springer, Cham, 2017). https://doi.org/10.1007/978-3-319-48933-9_16

14. C. Gao, L. Liu, J. Mater. Sci.: Mater. Electron. **28**, 14417–14423 (2017)

15. J. Li, J. Xu, W. Li, H. Shen, J. Mater. Sci.: Mater. Electron. **29**, 17503–17507 (2018)

16. Y.P. Venkata Subbaiah, P. Prathap, K.T.R. Reddy, D. Mangalaraj, K. Kim, J. Yi, J. Phys. D **40**, 3683–3688 (2007)

17. R. Mendil, Z. Ben Ayadi, C. Vázquez-Vázquez, M.A. López-Quintela, K. Djessas, J. Mater. Sci.: Mater. Electron. **29**, 10656–10662 (2018)

18. Y.P. Venkata Subbaiah, P. Prathap, K.T. Ramakrishna Reddy, R.W. Miles, J. Yi, Thin Solid Films **516**, 7060–7064 (2008)

19. A.A. Ojo, I.M. Dharmadasa, Sol. Energy **158**, 721–727 (2017)

20. R.G. Valeev, E.A. Romanov, V.L. Vorobiev, V.V. Mukhgalin, V.V. Kriventsov, A.I. Chukavin, B.V. Robouch, Mater. Res. Express **2**, 025006 (2015). https://doi.org/10.1088/2053-1591/2/2/025006

21. K.T. Ramakrishna Reddy, Y.V. Subbaiah, T.B.S. Reddy, D. Johnston, I. Forbes, R.W. Miles, Thin Solid Films **431–432**, 340–343 (2003)

22. C. Dhanemozhi, R. John, K.R. Murali, Mater. Today: Proc. **4**, 5185–5189 (2017)

23. P.S. Patil, Mater. Chem. Phys. **59**, 185–198 (1999)

24. Y.P. Venkata Subbaiah, K.T. Ramakrishna Reddy, Mater. Chem. Phys. **92**, 448–452 (2005)

25. S. Chandra, R.K. Pandey, Phys. Status Solidi (a) **73**, 415–454 (1982)

26. A.A. Yadav, M.A. Barote, E.U. Masumdar, Mater. Chem. Phys. **121**, 53–57 (2010)

27. A.A. Yadav, E.U. Masumdar, Mater. Res. Bull. **45**, 1455–1459 (2010)

28. N.M. Patil, S.G. Nilange, A.A. Yadav, Thin Solid Films **664**, 19–26 (2018)

29. C. Khelifi, A. Attaf, H. Saidi, A. Yahia, M. Dahnoun, A. Saadi, Optik—Int. J. Light Electron Opt. **127**, 11055–11062 (2016)

30. A.S. Rajbhoj, S.T. Gaikwad, J.T. Deshmukh, V.M. Bhuse, Arch. Appl. Sci. Res. **4**, 951–959 (2012)

31. R.N. Pandey, K.S. Chandra Babu, O.N. Srivastava, Prog. Surf. Sci. **52**, 125–192 (1996)

32. Y. Kuang, T. Yamada, K. Domen, Joule **1**, 290–305 (2017)

33. D.S. Ginley, M.A. Butler, Charge-transfer processes in photoelectrochemical cells, in *Photoeffects at Semiconductor-Electrolyte Interfaces, ACS Symposium Series*, ed. by A. Nozik (American Chemical Society: Washington, DC, 1981). https://doi.org/10.1021/bk-1981-0146.ch005

34. R.H. Wilson, Crit. Rev. Solid State Mater. Sci. **10**, 1–41 (1980)

35. P.P. Hankare, P.A. Chate, P.A. Chavan, D.J. Sathe, J. Alloys Compd. **461**, 623–627 (2008)

36. B. Iandolo, H. Zhang, B. Wickman, I. Zorić, G. Conibeer, A. Hellman, RSC Adv. **5**, 61021–61030 (2015)

37. A.A. Yadav, E.U. Masumdar, J. Alloys Compd. **509**, 5394–5399 (2011)

38. L.P. Deshmukh, V.S. Sawant, P.P. Hankare, Sol. Cells **31**, 549–557 (1991)

39. A.A. Yadav, E.U. Masumdar, Sol. Energy **84**, 1445–1452 (2010)

40. P.K. Mahapatra, A.R. Dubey, Sol. Energy Mater. Sol. Cells **32**, 29–35 (1994)

41. I.C. Kaya, S. Akin, H. Akyildiz, S. Sonmezoglu, Sol. Energy **169**, 196–205 (2018)

42. H.J. Moller, Prog. Mater. Sci. **35**, 205–418 (1991)

43. S. Das, K.C. Mandal, R.N. Bhattacharya, Chapter 2 earth-abundant Cu$_2$ZnSn(S,Se)$_4$ (CZTSSe) solar cells, in *Semiconductor Materials for Solar Photovoltaic Cells*, ed. by M.P. Paranthaman et al. (Springer, Cham, 2016). https://doi.org/10.1007/978-3-319-20331-7_2